# Accepted Manuscript


Design, synthesis and biological evaluations of N-Hydroxy thienopyrimidine-2,4-diones as inhibitors of HIV reverse transcriptase-associated RNase H

Jayakanth Kankanala, Karen A. Kirby, Andrew D. Huber, Mary C. Casey, Daniel J. Wilson, Stefan G. Sarafianos, Zhengqiang Wang

PII: S0223-5234(17)30769-9

DOI: 10.1016/j.ejmech.2017.09.054

Reference: EJMECH 9769

To appear in: *European Journal of Medicinal Chemistry*

Received Date: 24 August 2017

Revised Date: 13 September 2017

Accepted Date: 25 September 2017

Please cite this article as: J. Kankanala, K.A. Kirby, A.D. Huber, M.C. Casey, D.J. Wilson, S.G. Sarafianos, Z. Wang, Design, synthesis and biological evaluations of N-Hydroxy thienopyrimidine-2,4-diones as inhibitors of HIV reverse transcriptase-associated RNase H, *European Journal of Medicinal Chemistry* (2017), doi: 10.1016/j.ejmech.2017.09.054.

## Graphical abstract

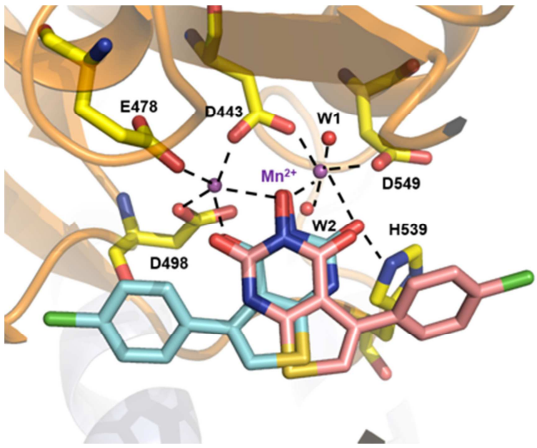


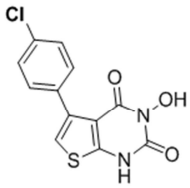


**11d**

$IC_{50}$ (RNase H) = 0.04 μM
$IC_{50}$ (RT pol) = >10 μM
$IC_{50}$ (IN) = 2.1 μM
$EC_{50}$ (HIV-1) = 7.4 μM
$CC_{50}$ > 100 μM

# Design, Synthesis and Biological Evaluations of N-Hydroxy thienopyrimidine-2,4-diones as Inhibitors of HIV Reverse Transcriptase-Associated RNase H

*Jayakanth Kankanala [1], Karen A. Kirby [2,3], Andrew D. Huber [2,4], Mary C. Casey [2,3], Daniel J. Wilson [1], Stefan G. Sarafianos [2,3,5] and Zhengqiang Wang*[1]*

[1] *Center for Drug Design, Academic Health Center, University of Minnesota, Minneapolis, MN 55455, USA*

[2] *Christopher S. Bond Life Sciences Center, University of Missouri, Columbia, Missouri, 65211, USA*

[3] *Department of Molecular Microbiology & Immunology, School of Medicine, University of Missouri, Columbia, Missouri, 65211, USA*

[4] *Department of Veterinary Pathobiology, College of Veterinary Medicine, University of Missouri, Columbia, Missouri, 65211, USA*

[5] *Department of Biochemistry, University of Missouri, Columbia, Missouri, 65211, USA*

## Abstract

Human immunodeficiency virus (HIV) reverse transcriptase (RT) associated ribonuclease H (RNase H) is the only HIV enzymatic function not targeted by current antiviral drugs. Although various chemotypes have been reported to inhibit HIV RNase H, few have shown significant antiviral activities. We report herein the design, synthesis and biological evaluation of a novel *N*-hydroxy thienopyrimidine-2,3-dione chemotype (**11**) which potently and selectively inhibited RNase H with considerable potency against HIV-1 in cell culture. Current structure-activity-relationship (SAR) identified analogue **11d** as a nanomolar inhibitor of RNase H ($IC_{50}$ = 0.04 µM) with decent antiviral potency ($EC_{50}$ = 7.4 µM) and no cytotoxicity ($CC_{50}$ > 100 µM). In extended biochemical assays compound **11d** did not inhibit RT polymerase (pol) while inhibiting integrase strand transfer (INST) with 53 fold lower potency ($IC_{50}$ = 2.1 µM) than RNase H

inhibition. Crystallographic and molecular modeling studies confirmed the RNase H active site binding mode.

**Keywords:** N-Hydroxy thienopyrimidine-2,4-diones; Human Immunodeficiency Virus (HIV); RNase H; integrase strand transfer; RT-Polymerase, molecular modeling and crystallography.

## Introduction

HIV infection remains a major epidemic and a global healthcare threat. As of 2015, an estimated 36.7 million people worldwide are living with HIV [1]. The standard therapy for HIV infection, highly active antiretroviral therapy (HAART) [2], consists of inhibitors of all three HIV encoded enzymes: protease, RT and integrase (IN). While HAART has proven to effectively suppress viral replication, the required long term HAART treatment can be plagued by adverse effects and drug resistance. This is precisely why even with a large number of FDA-approved drugs there is still a pressing need for improved antivirals, particularly those with novel and distinct mechanisms of action [3, 4] to combat drug resistance. Of all FDA-approved HIV drugs, inhibitors of RT comprise two distinct classes, nucleoside RT inhibitors (NRTIs) [5] and non-nucleoside RT inhibitors (NNRTIs) [6], and are of particular importance for HAART. RT has two distinct active sites: an N-terminal DNA pol active site and a C-terminal RNase H active site. Interestingly, currently known NRTIs and NNRTIs all target the DNA pol function of RT, and inhibitors of RT RNase H have yet to enter the development pipeline. Therefore, RT-associated RNase H represents a novel target for HIV drug development and provides an attractive approach to treating HIV strains resistant to current drugs [7-9].

The active site of RNase H features four carboxylic residues (DEDD) interacting with two metal ions ($Mg^{2+}$) in close proximity. Chemical inhibition of RNase H at the active site thus minimally entails a chelating triad capable of chelating the two $Mg^{2+}$ ions [3]. Several types of active site

inhibitors of RT-associated RNase H have been reported in the literature (Figure 1A). These include diketoacids (**1**) [10], 2-hydroxyisoquinoline-1,3-diones (HID, **2**) [11-13], hydroxylated tropolones (**3**) [14], pyrimidinol carboxylic acids (**4**) [3], hydroxypyridone carboxylic acids (**5**) [15], hydroxynaphthyridines (**6**) [16], and pyridopyrimidones (**7**) [17]. Notably, all these chemotypes feature a metal chelator and a peripheral hydrophobic moiety. A similar pharmacophore is required for the inhibition of HIV IN. Therefore, most reported RNase H inhibitors also tend to inhibit IN, making achievement of selective biochemical inhibition of HIV RNase H over IN challenging. We have long been interested in designing potent and selective RNase H inhibitors [12, 13, 15, 18-20] particularly with the HID (**2**) [12, 13] and 3-hydroxypyrimidine-2,4-dione (HPD) (**8**) [18-20] chemotypes. Hybridization of these two scaffolds led to the design of chemotype **9** (Figure 1B) which is similar to the *N*-hydroxyurea reported as an inhibitor type of flap endonuclease-1 [21]. Bioisosteric replacement of the phenyl ring of **9** with a thiophene ring yielded chemotypes **10** and **11** (Figure 1B). The latter (**11**) proved to inhibit RNase H potently and selectively in our biochemical assays and reduce viral replication significantly in our cell-based assay. We report herein the chemical synthesis, biochemical, antiviral and structural evaluations of inhibitor type **11**.

[Insert Figure 1 here]

**Results and Discussion**

**Chemistry.** The initial HID analogue **14** was prepared in two steps according to reported procedures (Scheme 1A) starting from iodohomophthalic acid (**12**) [12, 22, 23]. The introduction of the phenyl group was achieved *via* Suzuki coupling. The resulting diacid intermediate **13** was cyclized by treating with *O*-tetrahydropyran (THP) protected hydroxylamine in the presence of carbonyldiimidazole (CDI) followed by the deprotection of THP using p-toluenesulfonic acid (p-

TSA) to afford the desired product (**14**). The synthesis of scaffolds **9**, **19**, and **10** all featured a key base-promoted cyclization (step c) from an *ortho* amino ester intermediate (**16**, **18**, **20**, Scheme 1B–D) to construct the hydroxyurea moiety. The cyclization presumably involves three sequential events: first the amino group of the intermediate (*e.g.* **16**) reacted with CDI to form an imidazole urea intermediate; second, the imidazole ring of the urea intermediate was replaced by a protected hydroxylamine to form a hydroxyurea intermediate; and finally upon treatment of NaOH the deprotonated hydroxyurea reacted with the ortho ester group to produce cyclized hydroxyureas which upon deprotection afforded desired compounds of chemotypes **9**, **19**, and **10** (Scheme 1). The key intermediate **16** was synthesized via Suzuki coupling of arylboronic acid with methyl anthranilate (**15**). The intermediate **18** [24] was prepared by treating 1-benzyl-3-oxo-piperidine-4-carboxylic acid ethyl ester hydrochloride (**17**) with an excess amount of ammonium acetate in refluxing ethanol. Intermediates **20** are all commercially available.

[Insert Scheme 1 here]

The synthesis of chemotype **11** also involved a base-promoted cyclization (step b, Scheme 2) from *ortho* amino ester intermediates (**22**, **24** and **25**). Intermediates **22** and **24** were prepared *via* Gewald reaction [25, 26] which involves condensation of appropriate aldehydes (**20**) or ketones (**22**) with ethyl cyanoacetate in presence of an elemental sulfur and base (Scheme 2A). All intermediates **25** are commercially available.

[Insert Scheme 2 here]

**Biology.** All final compounds were first tested in a biochemical assay for inhibition against HIV RT-associated RNase H. HIV RNase H cleaves viral RNA at multiple stages of reverse transcription with at least three distinct modes [12]: random internal cleavages, DNA 3′ end-directed and polymerase dependent cleavages, and RNA 5′ end-directed cleavages. In the current

work our biochemical assay used the HTS-1 RNA/DNA substrate to specifically probe random internal cleavage, which is believed to be the dominant mode of RNA cutting. Importantly, due to the spatial and temporal relationship between the RNase H and pol domains [27], inhibition of RNase H is often accompanied by the inhibition of RT pol. In addition, RNase H shares a similar active site fold and mechanism of catalysis with HIV IN [28]. Therefore, we have included biochemical assays measuring the activity of RT pol and INST reactions to gauge the selectivity of our compounds toward RNase H inhibition. Finally, all analogues were also tested for cytotoxicity and antiviral potency in a cell-based MAGI assay [29]. Previously reported HIV RNase H inhibitor trihydroxybenzoyl naphthyl hydrazone (THBNH) [30] was used as control in all RT assays and the FDA-approved INSTI, dolutegravir (DTG) [31] was used as control in both the INST assay and the MAGI antiviral assay. The assay results are summarized in Table 1.

The current inhibitors were designed based on 6-phenyl HID (**14**), which inhibited both HIV RNase H and INST in low micromolar range without inhibiting RT pol. Replacing the $CH_2$ at position 4 of compound **14** yielded *N*-hydroxybenzo pyrimidine-2,4-diones **9a** and conferred a 6.5-fold increase in RNase H inhibition ($IC_{50}$ = 0.2 μM for **9a** *vs.* 1.3 μM for **14**) and a 5.5-fold decrease in INST inhibition ($IC_{50}$ = 11 μM for **9a** *vs.* 2.0 μM for **14**). These early data strongly suggest that potent and selective biochemical inhibition of RNase H can be achieved with chemotype **9**, though just like HID analogue **14**, both **9a** and **9b** exhibited severe cytotoxic ($CC_{50}$ = 6.0 μM and 9.9 μM, respectively) which likely accounts for their observed antiviral potencies ($EC_{50}$ = 3.8 μM and 4.5 μM, respectively). However, when the fused benzene ring of **9a** and **9b** is replaced with a nonaromatic piperidine ring, the resulting compound **19** did not demonstrate significant antiviral activity at concentrations up to 20 μM, which prompted us to further diversify the general hydroxyurea chemotypes **9** and **19**.

Toward this end, we pursued the replacement of the fused benzene ring with a bioisosteric thiophene ring. The thiophene replacement is particularly attractive due to the commercial availability of many *ortho* amino ester intermediates (**25**, Scheme 2B) or easy synthetic accessibility *via* Gewald reaction (Scheme 2A). The initial thiophene derivative **10a** displayed very similar biological profiles to **9a** and **9b** with potent RNase H inhibition ($IC_{50}$ = 0.10 μM), moderate INST inhibition ($IC_{50}$ = 4.5 μM), no RT pol inhibition and a moderate antiviral activity ($EC_{50}$ = 11 μM) that mostly reflects its cytotoxicity ($CC_{50}$ = 28 μM). Notably, halogen substitution at the 4′ position of the phenyl ring of **10** largely mitigated the cytotoxicity (**10b** and **10c**). Particularly interesting is compound **10c** which exhibited improved RNase H inhibition ($IC_{50}$ = 0.070 μM) along with substantially decreased INST inhibition ($IC_{50}$ = 23 μM), amounting to a more potent and selective RNase H inhibitory profile *in vitro* when compared to **9a** and **9b**. The lack of antiviral activity, however, remains a challenge. Interestingly, for bioisosteric replacement the fused thiophene ring can be placed such that the sulfur atom is either facing up (chemotype **10**) or facing down (chemotype **11**). When compared to **10a**, the isomeric **11a** displayed similar levels of biochemical inhibition against RNase H and INST. Introducing a flexible methylene group between the phenyl ring and the hydroxythieno pyrimidine-2,4-dione core (compound **11b**) further improved the RNase H inhibition ($IC_{50}$ = 0.043 μM). Significantly, when the phenyl ring is placed one position further removed from the sulfur atom (**11c** vs **11a**), moderate antiviral activity was observed ($EC_{50}$ = 14 μM) with no cytotoxicity ($CC_{50}$ > 100 μM). Biochemically, **11c** inhibited RNase H ($IC_{50}$ = 0.10 μM) and to a much lesser degree INST ($IC_{50}$ = 1.3 μM) but not RT pol ($IC_{50}$ > 10 μM). Introducing a chloro substituent at the 4′ position of the phenyl ring led to compound **11d** with exceptional inhibition against RNase H ($IC_{50}$ = 0.04 μM), increased antiviral activity ($EC_{50}$ = 7.4 μM) and no observed cytotoxicity at 100 μM.

Although **11d** also inhibited INST ($IC_{50}$ = 2.1 μM), its inhibition against RNase H was far more potent (53-fold) and it did not inhibit RT pol ($IC_{50}$ > 10 μM). To further assess the impact of thiophene ring substitutions on biochemical inhibitory profile and antiviral activity, several analogues involving simple alkyl substituents (**11e**–**g**), carboxylic acid (**11h**), cycloalkyl fused ring (**11i**–**j**) and piperidine fused (**11k**–**m**) were synthesized and evaluated. These analogues generally inhibited RT-RNase H in the nanomolar range ($IC_{50}$ = 0.10–0.30 μM) without inhibiting RT pol ($IC_{50}$ > 10 μM) and with moderate INST inhibition ($IC_{50}$ = 3.6–35 μM), except for **11k** which did not inhibit INST at 100 μM. Importantly, a few of these analogues (**11e**, **11g**, **11i** and **11j**) also showed significant antiviral activity in micromolar range ($EC_{50}$ = 7.4–22 μM). Overall, our data suggest that the hydroxythienopyrimidine-2,4-dione chemotype (**11**) represents a novel scaffold for designing potent and selective HIV RNase H inhibitors with antiviral activity. Compared to previously reported HID **14**, our best compound **11d** exhibited substantially improved potency and selectivity inhibiting RNase H *in vitro* and a much more favorable antiviral profile.

[Insert Table 1 here]

**Molecular Modeling.** Docking analysis was performed with Glide XP (version 6.4) [32, 33] using two metal sites as a constraint. The predicted binding mode of compound **11a** within the active site of RNase H suggests a potential interaction between the *N*-hydroxypyrimidine-2,4-dione (chelating triad) and the two metal cofactors ($Mg^{2+}$), which are coordinated to the conserved active site acidic residues D443, E478, D498, and D549. A similar binding mode was postulated for compound **11d**. Compound **11d** was predicted to bind in the active site of RNase H with two possible binding modes (Figure 2B and 2C). In both binding modes, an interaction between the *N*-hydroxy-pyrimidine-2,4-dione (chelating triad) and the two active site metal

cations (coordinated to essential active site residues D443, E478, D498, and D549) was predicted. The keto group at the 4-position of **11d** appears to form H-bonding interactions with H539, which would stabilize inhibitor positioning near the active site metal-chelating residues D443, E478, D498, and D549, all of which are crucial for RT-RNase H activity. In the top scoring pose of **11d** (magenta, Figure 2B**),** the 4-chlorophenyl at 5-position of the *N*-hydroxy-pyrimidine-2,4-dione core was predicted to have an edge-on π-stacking interaction between the chlorophenyl ring of the ligand and RNase H residue H539. This interaction may limit the conformational flexibility of the loop with H539 and thus impact the efficiency of RNase H catalytic activity. Notably, a similar binding mode was observed for RT complexes with dsDNA or RNA−DNA hybrids as reported by Harrison et.al [34] and Sarafianos et.al [35, 36]. In an alternate predicted binding mode of **11d** (blue, Figure 2C), the interaction of the chelating triad with the metal ions is intact but the 4-chlorophenyl ring flips to the other side of the binding pocket resulting in the loss of key interaction with H539. The Glide XP scores for the predicted binding modes of 11a and 11d was shown in Figure 2D. Ligands with the low score is predicted to have a better binding with the protein.

[Insert Figure 2 here]

**Crystal structure of HIV RT in complex with 11b.** In order to further understand the molecular details of HIV RT-associated RNase H inhibition by compounds of the *N*-hydroxy thienopyrimidine-2,3-dione chemotype, we solved the crystal structure of HIV RT in complex with analogue **11b**, at 1.8 Å resolution. The asymmetric unit comprises two RT molecules (Figure 3, middle panel), and therefore we were able to capture two distinct RNase H active sites in the same crystal structure, similar to previous reports [15, 38]. Importantly, analogue **11b** is bound at both of these sites and adopts a different conformation in each active site (Figure 3, top

and bottom panels). In both RNase H active sites, two $Mn^{2+}$ ions are bound by conserved active site residues D443, E478, D498, and D549. Analogue **11b** chelates both $Mn^{2+}$ ions through the hydroxyl and carbonyl groups of the pyrimidine ring. **11b** also interacts directly with RT in both RNase H active sites through interactions of a carbonyl group on the pyrimidine ring with RT residues H539 and D549 (Figure 3, top and bottom panels). In RNase H active site 1 (Figure 3, top panel), the thieno group points in the direction of H539, while in RNase H active site 2 (Figure 3, bottom panel), the same group points in the opposite direction. Multiple binding modes of an inhibitor at the HIV-1 RT RNase H active site have also recently been observed for a 2-hydroxyisoquinoline-1,3-dione analogue [38]. The lack of additional protein-inhibitor interactions and the observed multiple modes of inhibitor binding at the RNase H active site may contribute to the decreased antiviral activity of the *N*-hydroxy thienopyrimidine-2,3-dione compounds.

[Insert Figure 3 here]

**Conclusions**

Herein we report a series of novel *N*-hydroxy thienopyrimidine-2,3-diones, which potently and selectively inhibited RNase H in low sub-micromolar range and with considerable potency against HIV-1 in cell culture. While some of the analogues also inhibited INST, this inhibition was substantially less than that for RT RNase H inhibition, suggesting that the *N*-hydroxy thienopyrimidine-2,3-diones chemotype may represent an interesting scaffold for developing RNase H-specific inhibitors. Interestingly, many of these new analogues inhibited HIV-1 in cell culture at low micromolar concentrations. The best compound **11d** exhibited low nanomolar inhibition of RNase H ($IC_{50}$ = 0.04 µM) with considerable antiviral activity ($EC_{50}$ = 7.4 µM) and

no cytotoxicity ($CC_{50}$ > 100 μM). The active site-directed RNase H inhibition was further corroborated with molecular docking and crystallographic studies.

## Experimental

**Chemistry. General Procedures.** All commercial chemicals were used as supplied unless otherwise indicated. Flash chromatography was performed on a Teledyne Combiflash RF-200 with RediSep columns (silica) and indicated mobile phase. All moisture sensitive reactions were performed under an inert atmosphere of ultrapure argon with oven-dried glassware. $^{1}H$ and $^{13}C$ NMR spectra were recorded on a Varian 600 MHz and Bruker 400 spectrometer. Mass data were acquired on an Agilent TOF II TOS/MS spectrometer capable of ESI and APCI ion sources. Analysis of sample purity was performed on a Varian Prepstar SD-1 HPLC system with a Phenomenex Gemini, 5 μm C18 column (250 mm × 4.6 mm). HPLC conditions: solvent A = H2O, solvent B = MeCN; flow rate = 1.0 mL/min; compounds were eluted with a gradient of 5% MeCN/$H_2O$ for 0−5 min and to 95% MeCN/$H_2O$ from 5 to 30 min followed by 100% MeCN from 35 to 40 min. Purity was determined by total absorbance at 254 nm. The melting points (m.p.) were determined using an electro thermal Mel-Temp capillary melting point apparatus. All tested compounds have a purity ≥98%.

**2-Hydroxy-6-phenylisoquinoline-1,3(2H,4H)-dione (14)** [12, 23]**.** A solution of homophthalic acid (**13**, 1.0 equiv) and $NH_2OTHP$ (1.2 equiv) in toluene (10 mL) was refluxed for 5 min. To the mixture, a solution of CDI (1.0 equiv) in DCM was added dropwise. The suspension turned clear and stirred at reflux for 12 h, a black solid separated from solution and the TLC indicated the disappearance of starting material. The reaction mixture was cooled and passed through a short pad of silica gel which was then rinsed with (EtOAc/ hexane, 1:3), the combined filtrate was

evaporated to dryness. The product was used for the next reaction without further purification. The cyclized product was dissolved in MeOH (5.0 mL) and treated with pTSA hydrate (1.0 equiv) and stirred at room temperature for 2−3 h. Upon the disappearance of starting material by TLC, the mixture was evaporated to dryness to get pale-yellow solid. The solid obtained was triturated with water and then with ether and dried at room temperature to afford the desired product (**14**) as a colorless solid. Yield: 69%; m.p. 181-183 °C. $^{1}$H NMR (600 MHz, DMSO-$d_6$) δ 10.40 (s, 1H), 8.09 (d, $J$ = 8.2 Hz, 1H), 7.79 (d, $J$ = 8.2 Hz, 1H), 7.75 (d, $J$ = 7.6 Hz, 2H), 7.72 (s, 1H), 7.52 (t, $J$ = 7.6 Hz, 2H), 7.45 (t, $J$ = 7.3 Hz, 1H), 4.32 (s, 2H). $^{13}$C NMR (150 MHz, DMSO-$d_6$) δ 166.5, 161.7, 144.8, 138.6, 135.5, 129.3, 128.8, 128.5, 127.1, 125.9, 125.8, 124.1, 37.2. HRMS-ESI (−) *m/z* calculated for $C_{15}H_{10}NO_3$-, 252.0666 [M-H]-; found: 252.0667.

**General procedure for the cyclization of *ortho* amino esters and deprotection (9a-b, 19, 10a-c, 11a-m)** [21]**.** To a solution of *ortho* amino ester (1.0 eq) in toluene (0.1 M) was added CDI (1.25 equiv) and refluxed for 2 h. The THP or benzyl protected hydroxylamine (1.5 equiv) was then added and refluxing was continued for 1 h. The solution was concentrated, suspended in EtOH (5 mL) and treated with 2 M NaOH (5 mL) and refluxed for 1 h. The resultant solution was cooled and acidified with AcOH to precipitate the O-protected imide. The product was filtered, washed with water and ether and air dried. The product was sufficiently pure without any further purification for the next reaction. The deprotection of O-protected imide was carried out using standard procedures. The cyclized product was dissolved in MeOH (5.0 mL) and treated with pTSA hydrate (1.0 equiv) and stirred at room temperature for 2−3 h. The mixture was evaporated to dryness to get pale-yellow solid and the solid obtained was triturated with water and then with ether/methanol and dried at room temperature to afford the desired product

as a colorless solid. Benzyl deprotection was carried out using HBr in acetic acid and compound was isolated as described above.

**3-Hydroxy-7-phenylquinazoline-2,4(1H,3H)-dione (9a).** Yield: 52%; m.p. >250 °C. $^{1}$H NMR (600 MHz, DMSO-$d_6$) δ 11.61 (s, 1H), 10.59 (s, 1H), 8.01 (d, *J* = 8.2 Hz, 1H), 7.68 (d, *J* = 7.4 Hz, 2H), 7.55-7.52 (m, 3H), 7.47 (t, *J* = 7.3 Hz, 1H), 7.41 (s, 1H). $^{13}$C NMR (100 MHz, DMSO-$d_6$) δ 159.07, 148.68, 146.12, 138.66, 138.47, 129.07, 128.62, 127.70, 126.82, 121.17, 112.98, 112.75. HRMS-ESI (−) *m/z* calculated for $C_{14}H_9N_2O_3$-, 253.0619 [M-H]-; found: 253.0617.

**7-(4-Chlorophenyl)-3-hydroxyquinazoline-2,4(1H,3H)-dione (9b).** Yield: 60%; m.p. >250 °C. $^{1}$H NMR (600 MHz, DMSO-$d_6$) δ 11.63 (s, 1H), 10.61 (s, 1H), 8.01 (d, *J* = 8.2 Hz, 1H), 7.70 (d, *J* = 8.2 Hz, 2H), 7.59 (d, *J* = 8.2 Hz, 2H), 7.52 (d, *J* = 8.0 Hz, 1H), 7.39 (s, 1H). $^{13}$C NMR (150 MHz, DMSO-$d_6$) δ 159.3, 148.9, 145.0, 139.0, 137.6, 133.8, 129.4, 129.3, 128.9, 121.4, 113.5, 112.9. HRMS-ESI (−) *m/z* calculated for $C_{14}H_8ClN_2O_3$-, 287.0229 [M-H]-; found: 287.0228.

**7-Benzyl-3-hydroxyhexahydropyrido[3,4-d]pyrimidine-2,4(1H,3H)-dione hydrochloride (19).** Yield: 40%; m.p. >250 °C. $^{1}$H NMR (600 MHz, DMSO-$d_6$) δ 11.41 (s, 1H), 11.35 (s, 1H), 10.55 (s, 1H), 7.62-7.48 (m, 5H), 4.43 (s, 2H), 3.92-3.46 (m, 4H), 2.60 (s, 2H). HRMS-ESI (−) *m/z* calculated for $C_{14}H_{14}N_3O_3$-, 272.1041 [M-H]-; found: 272.1040.

**3-Hydroxy-6-phenylthieno [3,2-d]pyrimidine-2,4(1H,3H)-dione (10a).** Yield: 75%; m.p. >250 °C. $^{1}$H NMR (600 MHz, DMSO-$d_6$) δ 12.06 (s, 1H), 10.55 (s, 1H), 7.76 (d, *J* = 7.3 Hz, 2H), 7.51-7.46 (m, 3H), 7.22 (s, 1H). $^{13}$C NMR (150 MHz, DMSO-$d_6$) δ 155.9, 151.5, 149.6, 143.7, 132.0, 129.9, 129.4, 126.1, 112.8, 109.4. HRMS-ESI (−) *m/z* calculated for $C_{12}H_7N_2O_3S$-, 259.0183 [M-H]-; found: 259.0180.

**6-(4-Fluorophenyl)-3-hydroxythieno[3,2-d]pyrimidine-2,4(1H,3H)-dione (10b).** Yield: 44%; m.p. >250 °C. $^{1}$H NMR (600 MHz, DMSO-$d_6$) δ 12.07 (s, 1H), 10.54 (s, 1H), 7.90 – 7.78 (m, 2H), 7.34 (t, *J* = 8.6 Hz, 2H), 7.20 (s, 1H). $^{13}$C NMR (100 MHz, DMSO-$d_6$) δ 155.6, 150.1, 149.4, 143.6, 128.4, 128.3, 116.3, 116.1, 112.9, 109.4. HRMS-ESI (−) *m/z* calculated for $C_{12}H_6FN_2O_3S$-, 277.0089 [M-H]-; found: 277.0088.

**6-(4-Chlorophenyl)-3-hydroxythieno[3,2-d]pyrimidine-2,4(1H,3H)-dione (10c).** Yield: 50%; m.p. >250 °C. $^{1}$H NMR (600 MHz, DMSO-$d_6$) δ 12.10 (s, 1H), 10.56 (s, 1H), 7.80 (d, *J* = 8.3 Hz, 2H), 7.55 (d, *J* = 8.3 Hz, 2H), 7.25 (s, 1H). $^{13}$C NMR (150 MHz, DMSO-$d_6$) δ 155.8, 150.0, 149.6, 143.8, 131.0, 129.4, 127.9, 121.2, 113.5, 109.8. HRMS-ESI (−) *m/z* calculated for $C_{12}H_6ClN_2O_3S$-, 292.9793 [M-H]-; found: 292.9793.

**3-Hydroxy-6-phenylthieno[2,3-d]pyrimidine-2,4(1H,3H)-dione (11a).** Yield: 71%; m.p. >250 °C. $^{1}$H NMR (600 MHz, DMSO-$d_6$) δ 12.44 (s, 1H), 10.51 (s, 1H), 7.66 (d, *J* = 7.5 Hz, 2H), 7.61 (s, 1H), 7.42 (t, *J* = 7.5 Hz, 2H), 7.32 (t, *J* = 7.5 Hz, 1H). $^{13}$C NMR (150 MHz, DMSO-$d_6$) δ 156.3, 148.8, 148.2, 134.2, 132.6, 129.3, 128.1, 125.3, 118.0, 115.9. HRMS-ESI (−) *m/z* calculated for $C_{12}H_7N_2O_3S$-, 259.0183 [M-H]-; found: 259.0185.

**6-Benzyl-3-hydroxythieno[2,3-d]pyrimidine-2,4(1H,3H)-dione (11b).** Yield: 79%; m.p. >250 °C. $^{1}$H NMR (600 MHz, DMSO-$d_6$) δ 12.20 (s, 1H), 10.40 (s, 1H), 7.33 (t, *J* = 7.5 Hz, 2H), 7.28 (d, *J* = 7.5 Hz, 2H), 7.24 (t, *J* = 7.1 Hz, 1H), 6.94 (s, 1H), 4.08 (s, 2H). $^{13}$C NMR (150 MHz, DMSO-$d_6$) δ 156.3, 148.8, 148.1, 139.8, 135.9, 128.8, 128.7, 126.8, 119.3, 114.2, 35.1. HRMS-ESI (−) *m/z* calculated for $C_{13}H_9N_2O_3S$-, 273.0339 [M-H]-; found: 273.0341.

**3-Hydroxy-5-phenylthieno[2,3-d]pyrimidine-2,4(1H,3H)-dione (11c).** Yield: 67%; m.p. 239-241 °C. $^{1}$H NMR (600 MHz, DMSO-$d_6$) δ 12.40 (s, 1H), 10.36 (s, 1H), 7.45 (d, *J* = 6.7 Hz, 2H), 7.37-7.35 (m, 3H), 7.04 (s, 1H). $^{13}$C NMR (150 MHz, DMSO-$d_6$) δ 155.6, 150.3, 147.8, 138.3,

134.4, 131.9, 128.7, 127.1, 114.6, 110.9. HRMS-ESI (−) *m/z* calculated for $C_{12}H_7N_2O_3S$-, 259.0183 [M-H]-; found: 259.0181.

**5-(4-Chlorophenyl)-3-hydroxythieno[2,3-d]pyrimidine-2,4(1H,3H)-dione (11d).** Yield: 60%; m.p. >250 °C. $^1$H NMR (600 MHz, DMSO-$d_6$) δ 12.42 (s, 1H), 10.38 (s, 1H), 7.48 (d, $J$ = 8.3 Hz, 2H), 7.43 (d, $J$ = 8.3 Hz, 2H), 7.09 (s, 1H). $^{13}$C NMR (100 MHz, DMSO-$d_6$) δ 155.9, 150.6, 148.2, 137.1, 133.4, 132.1, 130.8, 127.4, 115.4, 111.0. HRMS-ESI (−) *m/z* calculated for $C_{12}H_6ClN_2O_3S$-, 292.9793 [M-H]-; found: 292.9795.

**3-Hydroxythieno[2,3-d]pyrimidine-2,4(1H,3H)-dione (11e).** Yield: 85%; m.p. >250 °C. $^1$H NMR (600 MHz, DMSO-$d_6$) δ 12.30 (s, 1H), 10.43 (s, 1H), 7.16-7.13 (m, 2H). $^{13}$C NMR (150 MHz, DMSO-$d_6$) δ 156.0, 148.6, 148.4, 121.8, 117.5, 114.5. HRMS-ESI (−) *m/z* calculated for $C_6H_3N_2O_3S$-, 182.9870 [M-H]-; found: 182.9874.

**3-Hydroxy-5-methylthieno[2,3-d]pyrimidine-2,4(1H,3H)-dione (11f).** Yield: 80%; m.p. >250 °C. $^1$H NMR (600 MHz, DMSO-$d_6$) δ 12.23 (s, 1H), 10.34 (s, 1H), 6.71 (s, 1H), 2.35 (s, 3H). $^{13}$C NMR (150 MHz, DMSO-$d_6$) δ 156.60, 149.48, 148.39, 133.68, 112.64, 112.10, 15.4. HRMS-ESI (−) *m/z* calculated for $C_7H_5N_2O_3S$-, 197.0026 [M-H]-; found: 197.0027.

**3-Hydroxy-5,6-dimethylthieno[2,3-d]pyrimidine-2,4(1H,3H)-dione (11g).** Yield: 77%; m.p. >250 °C. $^1$H NMR (600 MHz, DMSO-$d_6$) δ 12.12 (s, 1H), 10.29 (s, 1H), 2.26 (s, 3H), 2.25 (s, 3H). $^{13}$C NMR (150 MHz, DMSO-$d_6$) δ 156.8, 148.5, 146.7, 128.6, 122.9, 113.1, 12.6, 11.9. HRMS-ESI (−) *m/z* calculated for $C_8H_7N_2O_3S$-, 211.0183 [M-H]-; found: 211.0182.

**3-Hydroxy-5-methyl-2,4-dioxo-1,2,3,4-tetrahydrothieno[2,3-d]pyrimidine-6-carboxylic acid (11h).** Yield: 52%; m.p. 237-239 °C. $^1$H NMR (600 MHz, DMSO-$d_6$) δ 13.23 (s, 1H), 12.50 (s, 1H), 10.47 (s, 1H), 2.72 (s, 3H). $^{13}$C NMR (150 MHz, DMSO-$d_6$) δ 162.8, 156.4, 151.2, 147.8,

143.0, 117.9, 113.6, 13.8. HRMS-ESI (−) *m/z* calculated for $C_8H_5N_2O_5S$-, 240.9925 [M-H]-; found: 240.9927.

**3-Hydroxy-1,5,6,7-tetrahydro-2H-cyclopenta[4,5]thieno[2,3-d]pyrimidine-2,4(3H)-dione (11i).** Yield: 64%; m.p. >250 °C. $^1$H NMR (600 MHz, DMSO-$d_6$) δ 12.19 (s, 1H), 10.35 (s, 1H), 2.81-2.79 (m, 4H), 2.42 – 2.28 (m, 2H). $^{13}$C NMR (100 MHz, DMSO-$d_6$) δ 156.1, 151.7, 148.6, 139.7, 130.8, 109.5, 28.2, 28.1, 27.3. HRMS-ESI (−) *m/z* calculated for $C_9H_7N_2O_3S$-, 223.0183 [M-H]-; found: 223.0185.

**3-Hydroxy-5,6,7,8-tetrahydrobenzo[4,5]thieno[2,3-d]pyrimidine-2,4(1H,3H)-dione (11j).** Yield: 69%; m.p. 241-243 °C. $^1$H NMR (600 MHz, DMSO-$d_6$) δ 12.14 (s, 1H), 10.30 (s, 1H), 2.76-2.75 (m, 2H), 2.61-2.60 (m, 2H), 1.76-1.71 (m, 4H).$^{13}$C NMR (150 MHz, DMSO-$d_6$) δ 156.3, 148.3, 147.0, 130.6, 125.7, 112.1, 24.7, 23.6, 22.4, 21.3. HRMS-ESI (−) *m/z* calculated for $C_{10}H_9N_2O_3S$-, 237.0339 [M-H]-; found: 237.0338.

**7-Ethyl-3-hydroxy-5,6,7,8-tetrahydropyrido[4',3':4,5]thieno[2,3-d]pyrimidine-2,4(1H,3H)-dione hydrochloride (11k).** Yield: 48%; m.p. >250 °C. $^1$H NMR (600 MHz, DMSO-$d_6$) δ 12.48 (s, 1H), 10.98 (s, 1H), 10.46 (s, 1H), 4.50-4.49 (m, 1H), 4.20-4.19 (m, 1H), 3.67-3.65 (m, 1H), 3.25-3.15 (m, 5H), 1.31 (t, $J$ = 7.2 Hz, 3H).$^{13}$C NMR (150 MHz, DMSO-$d_6$) δ 156.9, 149.9, 149.0, 129.0, 118.5, 111.9, 50.7, 48.4, 48.3, 22.9, 9.7. HRMS-ESI (−) *m/z* calculated for $C_{11}H_{12}N_3O_3S$-, 266.0605 [M-H]-; found: 266.0606 (free base).

**3-Hydroxy-5,6,7,8-tetrahydropyrido[4',3':4,5]thieno[2,3-d]pyrimidine-2,4(1H,3H)-dione hydrobromide (11l).** Yield: 69%; m.p. >250 °C. $^1$H NMR (600 MHz, DMSO-$d_6$) δ 12.34 (s, 1H), 10.45 (s, 1H), 9.17 (s, 2H), 4.26 (s, 2H), 3.39-3.37 (m, 2H), 3.05-3.04 (m, 2H). $^{13}$C NMR (150 MHz, DMSO-$d_6$) δ 156.8, 149.4, 148.9, 128.9, 118.6, 111.9, 41.6, 40.6, 22.6. HRMS-ESI (−) *m/z* calculated for $C_9H_8N_3O_3S$-, 238.0292 [M-H]-; found: 238.0288 (free base).

**7-Benzyl-3-hydroxy-5,6,7,8-tetrahydropyrido[4',3':4,5]thieno[2,3-d]pyrimidine-2,4(1H,3H)-dione hydrochloride (11m).** Yield: 79%; m.p. >250 °C. $^{1}$H NMR (600 MHz, DMSO-$d_6$) δ 12.47 (s, 1H), 11.51 (s, 1H), 10.46 (s, 1H), 7.65-7.62 (m, 2H), 7.47-7.44 (m, 3H), 4.50-4.44 (m, 2H), 4.22 (s, 2H), 3.66-3.64 (m, 2H), 3.18-3.17 (m, 2H). $^{13}$C NMR (150 MHz, DMSO-$d_6$) δ 156.1, 149.0, 148.2, 131.1, 129.3, 128.6, 128.2, 117.3, 111.0, 57.6, 47.8, 47.7, 22.0. HRMS-ESI (−) *m/z* calculated for $C_{16}H_{14}N_3O_3S$-, 328.0761 [M-H]-; found: 328.0762 (free base).

## Biology

### Reagents

***Biologicals***. Recombinant HIV-1 reverse transcriptase (RT) was expressed and purified as previously described [39]. P4R5 HIV infection indicator cells were obtained from the NIH AIDS Reagent Program, Division of AIDS, NIAID, NIH (p4R5.MAGI from Dr. Nathaniel Landau). These cells express CD4, CXCR4 and CCR5 as well as a β-galactosidase reporter gene under the control of an HIV LTR promoter.

***Chemicals.*** DNA and RNA oligonucleotides for the preparation of RNA/DNA duplexes for assay of RNase H activity were purchased from Trilink (San Diego, CA).

***RNH assay.*** RNH activity was measured essentially as previously described [40]. Full-length HIV RT was incubated with the RNA/DNA duplex substrate HTS-1 (RNA 5'-gaucugagccugggagcu-3'-fluorescein annealed to DNA 3'-CTAGACTCGGACCCTCGA-5'-Dabcyl), a high sensitivity duplex that assesses non-specific internal cleavage of the RNA strand, in the presence of various concentrations of compound. Results were analyzed using Prism

software (GraphPad Software, San Diego, CA) for nonlinear regression to fit dose-response data to logistic curve models.

***RT polymerase assay.*** RT pol assays were carried out in 96-well plates by measuring the extension of an 18 nucleotide DNA primer (5'-GTCACTGTTCGAGCACCA-3') annealed to a 100 nucleotide DNA template (5'-ATGTGTGTGCCCGTCTGTTGTGTGACTCTGGTAACTAGAGATCCCTCAGACCCTTTTAGTCAGTGTGGAATATCTCATAGCTTGGTGCTCGAACAGTGAC-3'). Reactions containing 20 nM RT, 40 nM template/primer, and 10 μM deoxynucleotide triphosphates (dNTPs) in a buffer containing 50 mM Tris (pH 7.8) and 50 mM NaCl were initiated by the addition of 6 mM $MgCl_2$. Reactions contained 1% DMSO and increasing concentrations of compounds. DNA synthesis was carried out for 30 min at 37 °C, and reactions were arrested by the addition of 100 mM EDTA. The QuantiFluor dsDNA System (Promega) was used to quantify the amount of formed double-stranded DNA. Reactions were read at ex/em 504/531 nm in a PerkinElmer EnSpire Multilabel plate reader. Results were analyzed using Prism software (GraphPad Software, San Diego, CA) for nonlinear regression to fit dose-response data to logistic curve models [20, 41].

***HIV IN assay.*** HIV integrase was expressed and purified as previously reported [42]. Inhibition assays were performed using a modified protocol of our reported method [42]. Briefly, 2.1 μL of compound suspended in DMSO was placed in duplicate into a black 96 well non-binding plate (corning 3991). Compounds were plated in duplicate to a final concentration of 0.13 — 100 μM. To each well of the plate, 186.9 μL of reaction mixture without DNA substrate was added (10 mM HEPES pH 7.5, 10 % glycerol w/v, 10 mM $MnCl_2$, 1 mM DTT, 1 μM integrase). The

enzyme was incubated with inhibitor for 10 min at 25 °C after which the reaction was initiated by the addition of 21 µL of 500 nM oligo (5'-biotin-ATGTGGAAAATCTCTAGCA annealed with ACTGCTAGAGATTTTCCACAT-3'-Cy5). Reactions were incubated at 37 °C for 30 min and then quenched by the addition of 5.2 µL 500 mM EDTA. Each reaction was moved (200 µL) to a MultiScreen HTS PCR plate (Millipore MSSLBPC10) containing 20 µL streptavidin agarose beads (Life Technologies S951) and incubated with shaking for 30 min. A vacuum manifold was used to remove the reaction mixture and the beads were similarly washed 3 times with wash buffer (.05% SDS, 1 mM EDTA in PBS). The plates were further washed 3 times with 200 µL 50 mM NaOH to denature DNA not covalently linked to the biotin modification. For each denaturation step the plate was incubated with shaking at 25 °C for 5 min and the NaOH was removed by centrifugation at 1000 g for 1 min. The reaction products were eluted from the beads by the addition of 150 µL formamide. The plate was incubated at 25 °C for 10 min and read directly at 635/675 in a SpectraMax i3 plate reader (Molecular Devices).

***Antiviral assays.*** MAGI assays were carried out using P4R5 indicator cells essentially as previously described [29]. P4R5 cells were cultured in 96-well microplates with $4 \times 10^3$ cells per well and maintained in DMEM/10% FBS supplemented with puromycin (1 µg/mL). Cells were incubated with either 1% DMSO or varying concentrations of the drugs for 24 h and then exposed to HIV-1 (MOI of 1.25) followed by an additional incubation period of 48 h. The extent of infection was assessed using a fluorescence-based β-galactosidase detection assay, as previously described with minor modifications [43]. After the 48 h incubation period, cells were lysed and 4-methylumbelliferylgalactoside (MUG) substrate was added. The β-galactosidase produced during infection acts on the MUG substrate and yields a fluorescent product, 4-

methylumbelliferone (4-MU) that can be detected fluorimetrically with excitation wavelength 365 nm and emission wavelength 446 nm.

***Modeling and docking analysis.*** Molecular modeling was performed using the Schrödinger small molecule drug discovery suite 2014-3. The crystal structure of a hydroxypyridone carboxylic acid active-site RNase H inhibitor in complex with HIV Reverse Transcriptase was extracted from the Protein Data Bank (PDB code 5J1E) [37] as reported by Kankanala et.al [15]. The above structure was subjected to analysis and found that the native ligand, hydroxypyridone carboxylic acid was bound to the active site of RNase H. This model was subjected to Protein Preparation Wizard (Schrödinger Inc.) [44, 45] in which missing hydrogens atoms were added, zero-order bonds to metals were created followed by the generation of metal binding states. The structure of protein was minimized using OPLS 2005 force field [46] to optimize hydrogen bonding network and converge heavy atoms to an rmsd of 0.3 Å. The processed model indicates that the interaction between the hydroxypyridone carboxylic acid and RNase H is mediated by two metal cations ($Mg^{2+}$) coordinated by the active site residues D443, E478, D498, and D549. The receptor grid generation tool in Maestro (Schrödinger Inc.) was used to define an active site around the native ligand to cover all the residues within 12 Å from it with both the metal cofactors ($Mg^{2+}$) as a constraint to identify the chelating triad during docking. Compounds **11a** and **11d** were drawn using Maestro and subjected to Lig Prep [47] to generate conformers, possible protonation at pH of 7 ± 3, and metal binding states that serve as an input for docking process. All the dockings were performed using Glide XP (Glide, version 6.4) [32, 33] mode with both the $Mg^{2+}$ metal cofactors as a constraint. The van der Waals radii of nonpolar atoms for each of the ligands were scaled by a factor of 0.8. The predicted binding mode of compounds **11a** and **11d** features the critical interaction between the chelating triad and to the divalent metal

cofactors. All the ligands within the active site of RNase H were further refined post docking by minimizing under implicit solvent to account for the local protein flexibility.

***HIV-1 RT crystallization and data collection.*** HIV-1 RT containing C280S mutations in the p66 and p51 subunits was expressed and purified as previously described [48, 49]. Co-crystallization of HIV-1 RT with **11b** was accomplished by mixing a solution of RT at a final concentration of 11 mg/ml, 10 mM $MnCl_2$, 5 mM tris(2-carboxyethyl)phosphine (TCEP) HCl, 0.5% β-octylglucoside (BOG), and 1 mM **11b** in a 1:1 ratio with a solution of 15% PEG 3500, 0.1 M sodium potassium phosphate, 5% ethylene glycol, and 0.1 M Tris pH 6.5. Large, blocky crystals grew by hanging drop vapor diffusion at 18 °C in 2-3 days.

HIV-1 RT/**11b** co-crystals were additionally soaked with 1.5 mM **11b**, 5 mM TCEP HCl, 0.5% BOG, 8% ethylene glycol, and 10 mM $MnCl_2$ for 20 minutes before brief cryoprotection in a solution containing 23.5% ethylene glycol and 4% trimethylamine N-oxide, followed by fast cryo-cooling in liquid nitrogen. Two data sets collected at Beamline 23-ID-D of the Advanced Photon Source at Argonne National Laboratory were processed, scaled, and merged to 1.8 Å resolution using xia2 [50, 51]. The HIV-1 RT/**11b** crystals were of space group P1, and had unit cell dimensions of $a$ = 70.4 Å, $b$ = 89.1 Å, $c$ = 112.7 Å and $\alpha$ = 105.7°, $\beta$ = 95.0°, $\gamma$ = 110.7°. Two RT molecules were present in the asymmetric unit, and the Matthews coefficient was 2.7 $Å^3$/Da, corresponding to a solvent content of 53.8% [52]. Crystal data and statistics are listed in SI Table 1.

***Phase determination and structure refinement.*** The structure was determined by molecular replacement using the MrBump pipeline [53, 54], which used PDB ID 4KFB as the initial search model [55]. Buccaneer was used for initial model building [56, 57], and several cycles of model building and refinement were carried out using Coot [58] and Phenix [59] or Refmac [60, 61]

respectively. The final RT/**11b** structure was validated using MolProbity [62] Final refinement statistics are listed in SI Table 1.

**Acknowledgements**

This research was supported in part by the National Institutes of Health (AI100890 to SGS and ZW), and by the Research Development and Seed Grant Program of the Center for Drug Design, University of Minnesota. Use of the Advanced Photon Source, an Office of Science User Facility operated for the U.S. Department of Energy (DOE) Office of Science by Argonne National Laboratory, was supported by the U.S. DOE under Contract No. DE-AC02-06CH11357. We also thank Drs. Michail Isupov and Ronan Keegan of BioMEX Solutions, Inc. for assistance with structure solution and refinement.

**Appendix A. Supplementary data**

Chemical synthesis, general procedures, spectral data, including $^{1}$H NMR of intermediates (**13, 16a-b, 18, 22a-b, 24a-b, 25i**), and crystallographic data and refinement statistics are available in the supporting information. This material is available free of charge via the Internet at http://dx.doi.org/10.1016/j.ejmech.2016.12.030.

**PDB ID.** The atomic coordinates and structure factors have been deposited in the RCSB Protein Data Bank (PDB ID: 6AOC). Authors will release the atomic coordinates and experimental data upon article publication.

**AUTHOR INFORMATION**

**Corresponding Author**

Email: wangx472@umn.edu; Phone: +1 (612) 626-7025.

**Abbreviations**

| | |
|---|---|
| HIV | human immunodeficiency virus |
| RT | reverse transcriptase |
| RNase H | ribonuclease H |
| SAR | structure-activity-relationship |
| INST | integrase strand transfer |
| Pol | polymerase |
| NNRTI | nonnucleoside RT inhibitor |
| HAART | highly active antiretroviral therapy |
| NRTI | nucleoside reverse transcriptase inhibitor |
| HID | 2-hydroxyisoquinoline-1,3-dione |
| HPD | 3-Hydroxypyrimidine-2,4-dione |
| CDI | carbonyldiimidazole |
| MW | microwave |
| dNTP | deoxynucleotide triphosphate |
| MUG | 4-methylumbelliferyl-galactoside |
| 4-MU | 4-methylumbelliferone |

TCEP tris(2-carboxyethyl)phosphine

**References**

[1] https://www.aids.gov/hiv-aids-basics/hiv-aids-101/global-statistics/index.html.

[2] H. Fuji, E. Urano, Y. Futahashi, M. Hamatake, J. Tatsumi, T. Hoshino, Y. Morikawa, N. Yamamoto, J. Komano, Derivatives of 5-nitro-furan-2-carboxylic acid carbamoylmethyl ester inhibit RNase H activity associated with HIV-1 reverse transcriptase., J. Med. Chem., 52 (2009) 1380-1387.

[3] T.A. Kirschberg, M. Balakrishnan, N.H. Squires, T. Barnes, K.M. Brendza, X.W. Chen, E.J. Eisenberg, W.L. Jin, N. Kutty, S. Leavitt, A. Liclican, Q. Liu, X.H. Liu, J. Mak, J.K. Perry, M. Wang, W.J. Watkins, E.B. Lansdon, RNase H active site inhibitors of human immunodeficiency virus type 1 reverse transcriptase: design, biochemical activity, and structural information., J. Med. Chem., 52 (2009) 5781-5784.

[4] D.W. Kang, Y.N. Song, W.M. Chen, P. Zhan, X.Y. Liu, "Old dogs with new tricks": exploiting

alternative mechanisms of action and new drug design strategies for clinically validated HIV targets, Mol. Biosyst., 10 (2014) 1998-2022.

[5] T. Cihlar, A.S. Ray, Nucleoside and nucleotide HIV reverse transcriptase inhibitors: 25 years after zidovudine, Antiviral Res., 85 (2010) 39-58.

[6] M.P. de Bethune, Non-nucleoside reverse transcriptase inhibitors (NNRTIs), their discovery, development, and use in the treatment of HIV-1 infection: A review of the last 20 years (1989-2009), Antiviral Res., 85 (2010) 75-90.

[7] F. Yu, X.Y. Liu, P. Zhan, E. De Clercq, Recent advances in the research of HIV-1 RNase H

inhibitors, Mini. Rev. Med. Chem., 8 (2008) 1243-1251.

[8] L.L. Cao, W.G. Song, E. De Clercq, P. Zhan, X.Y. Liu, Recent Progress in the Research of Small Molecule HIV-1 RNase H Inhibitors, Curr. Med. Chem., 21 (2014) 1956-1967.

[9] X. Wang, P. Gao, L. Menendez-Arias, X. Liu, P. Zhan, Update on recent developments in small

molecular HIV-1 RNase H inhibitors (2013-2016): opportunities and challenges, Curr. Med. Chem., (2017).

[10] C.A. Shaw-Reid, V. Munshi, P. Graham, A. Wolfe, M. Witmer, R. Danzeisen, D.B. Olsen, S.S. Carroll, M. Embrey, J.S. Wai, M.D. Miller, J.L. Cole, D.J. Hazuda, Inhibition of HIV-1 ribonuclease H by a novel diketo acid, 4- 5-(benzoylamino)thien-2-yl -2,4-dioxobutanoic acid, J. Biol. Chem., 278 (2003) 2777-2780.

[11] K. Klumpp, J.Q. Hang, S. Rajendran, Y.L. Yang, A. Derosier, P.W.K. In, H. Overton, K.E.B.

Parkes, N. Cammack, J.A. Martin, Two-metal ion mechanism of RNA cleavage by HIV RNase H and mechanism-based design of selective HIV RNase H inhibitors, Nucleic Acids Res., 31 (2003) 6852-6859.

[12] S.K.V. Vernekar, Z. Liu, E. Nagy, L. Miller, K.A. Kirby, D.J. Wilson, J. Kankanala, S.G. Sarafianos, M.A. Parniak, Z.Q. Wang, Design, synthesis, biochemical, and antiviral evaluations of C6 benzyl and C6 biarylmethyl substituted 2-hydroxylisoquinoline-1,3-diones: dual inhibition against HIV reverse transcriptase-associated RNase H and polymerase with antiviral activities., J. Med. Chem., 58 (2015) 651-664.

[13] V.S. Tang J, Chen YL, Miller L, Huber AD, Myshakina N, Sarafianos SG, Parniak MA, Wang

Z., Synthesis, biological evaluation and molecular modeling of 2-Hydroxyisoquinoline-1,3-dione analogues as inhibitors of HIV reverse transcriptase associated ribonuclease H and polymerase., Eur. J. Med. Chem., 133 (2017) 85-96.

[14] D.M. Himmel, K.A. Maegley, T.A. Pauly, J.D. Bauman, K. Das, C. Dharia, A.D. Clark, K. Ryan, M.J. Hickey, R.A. Love, S.H. Hughes, S. Bergqvist, E. Arnold, Structure of HIV-1 reverse transcriptase with the inhibitor beta-thujaplicinol bound at the RNase H active site, Structure, 17 (2009) 1625-1635.

[15] J. Kankanala, K.A. Kirby, F. Liu, L. Miller, E. Nagy, D.J. Wilson, M.A. Parniak, S.G. Sarafianos, Z.Q. Wang, Design, synthesis, and biological evaluations of hydroxypyridonecarboxylic acids as inhibitors of HIV reverse transcriptase associated RNase H., J. Med. Chem., 59 (2016) 5051-5062.

[16] P.D. Williams, D.D. Staas, S. Venkatraman, H.M. Loughran, R.D. Ruzek, T.M. Booth, T.A. Lyle, J.S. Wai, J.P. Vacca, B.P. Feuston, L.T. Ecto, J.A. Flynn, D.J. DiStefano, D.J. Hazuda, C.M. Bahnck, A.L. Himmelberger, G. Dornadula, R.C. Hrin, K.A. Stillmock, M.V. Witmer, M.D. Miller, J.A. Grobler, Potent and selective HIV-1 ribonuclease H inhibitors based on a 1-hydroxy-1,8-naphthyridin-2(1H)-one scaffold, Bioorg. Med. Chem. Lett., 20 (2010) 6754-6757.

[17] G.L. Beilhartz, M. Ngure, B.A. Johns, F. DeAnda, P. Gerondelis, M. Gotte, Inhibition of the ribonuclease H activity of HIV-1 reverse transcriptase by GSK5750 correlates with slow enzyme-inhibitor dissociation, J. Biol. Chem., 289 (2014) 16270-16277.

[18] J. Tang, F. Liu, E. Nagy, L. Miller, K.A. Kirby, D.J. Wilson, B.L. Wu, S.G. Sarafianos, M.A.

Parniak, Z. Wang, 3-Hydroxypyrimidine-2,4-diones as selective active site inhibitors of HIV reverse transcriptase-associated RNase H: design, synthesis, and biochemical evaluations, J. Med. Chem., 59 (2016) 2648-2659.

[19] B.L. Wu, J. Tang, D.J. Wilson, A.D. Huber, M.C. Casey, J. Ji, J. Kankanala, J.S. Xie, S.G. Sarafianos, Z.Q. Wang, 3-Hydroxypyrimidine-2,4-dione-5-N-benzylcarboxamides potently inhibit HIV-1 integrase and RNase H, J. Med. Chem., 59 (2016) 6136-6148.

[20] J. Tang, K.A. Kirby, A.D. Huber, M.C. Casey, J. Ji, D.J. Wilson, S.G. Sarafianos, Z.Q. Wang,

6-Cyclohexylmethyl-3-hydroxypyrimidine-2,4-dione as an inhibitor scaffold of HIV reverase transcriptase: impacts of the 3-OH on inhibiting RNase H and polymerase, Eur. J. Med. Chem., 128 (2017) 168-179.

[21] L.N. Tumey, D. Bom, B. Huck, E. Gleason, J.M. Wang, D. Silver, K. Brunden, S. Boozer, S.

Rundlett, B. Sherf, S. Murphy, T. Dent, C. Leventhal, A. Bailey, J. Harrington, Y.L. Bennani, The identification and optimization of a N-hydroxy urea series of flap endonuclease 1 inhibitors, Bioorg. Med. Chem. Lett., 15 (2005) 277-281.

[22] J. Kankanala, C. Marchand, M. Abdelmalak, H. Aihara, Y. Pommier, Z.Q. Wang,

Isoquinoline-1,3-diones as selective inhibitors of tyrosyl DNA phosphodiesterase II (TDP2), J. Med. Chem., 59 (2016) 2734-2746.

[23] Y.L. Chen, J. Tang, M.J. Kesler, Y.Y. Sham, R. Vince, R.J. Geraghty, Z.Q. Wang, The design,

synthesis and biological evaluations of C-6 or C-7 substituted 2-hydroxyisoquinoline-1,3-diones as inhibitors of hepatitis C virus, Bioorg. Med. Chem., 20 (2012) 467-479.

[24] M.C. Lanier, M. Feher, N.J. Ashweek, C.J. Loweth, J.K. Rueter, D.H. Slee, J.P. Williams, Y.F. Zhu, S.K. Sullivan, M.S. Brown, Selection, synthesis, and structure-activity relationship of tetrahydropyrido 4,3-dipyrimidine-2,4-diones as human GnRH receptor antagonists, Bioorg. Med. Chem., 15 (2007) 5590-5603.

[25] D. Briel, A. Rybak, C. Kronbach, K. Unverferth, Substituted 2-aminothiopen-derivatives: a potential new class of GluR6-antagonists, Eur. J. Med. Chem., 45 (2010) 69-77.

[26] N.A. Osman, A. Ligresti, C.D. Klein, M. Allara, A. Rabbito, V. Di Marzo, K.A. Abouzid, A.H. Abadi, Discovery of novel tetrahydrobenzo b thiophene and pyrrole based scaffolds as potent and selective CB2 receptor ligands: the structural elements controlling binding affinity, selectivity and functionality, Eur. J. Med. Chem., 122 (2016) 619-634.

[27] G.L. Beilhartz, M. Gotte, HIV-1 ribonuclease H: structure, catalytic mechanism and inhibitors, Viruses-Basel, 2 (2010) 900-926.

[28] M. Nowotny, Retroviral integrase superfamily: the structural perspective, EMBO Rep., 10 (2009) 144-151.

[29] V.R. Sirivolu, S.K.V. Vernekar, T. Ilina, N.S. Myshakina, M.A. Parniak, Z.Q. Wang, Clicking

3 '-azidothymidine into novel potent inhibitors of human immunodeficiency virus, J. Med. Chem., 56 (2013) 8765-8780.

[30] D.M. Himmel, S.G. Sarafianos, S. Dharmasena, M.M. Hossain, K. McCoy-Simandle, T. Ilina,

A.D. Clark, J.L. Knight, J.G. Julias, P.K. Clark, K. Krogh-Jespersen, R.M. Levy, S.H. Hughes, M.A. Parniak, E. Arnold, HIV-1 reverse transcriptase structure with RNase H

inhibitor dihydroxy benzoyl naphthyl hydrazone bound at a novel site, ACS Chem. Biol., 1 (2006) 702-712.

[31] B.A. Johns, T. Kawasuji, J.G. Weatherhead, T. Taishi, D.P. Temelkoff, H. Yoshida, T. Akiyama, Y. Taoda, H. Murai, R. Kiyama, M. Fuji, N. Tanimoto, J. Jeffrey, S.A. Foster, T. Yoshinaga, T. Seki, M. Kobayashi, A. Sato, M.N. Johnson, E.P. Garvey, T. Fujiwara, Carbamoyl pyridone HIV-1 integrase inhibitors 3. a diastereomeric approach to chiral nonracemic tricyclic ring systems and the discovery of dolutegravir (S/GSK1349572) and (S/GSK1265744), J. Med. Chem., 56 (2013) 5901-5916.

[32] Small-Molecule Drug Discovery Suite 2014-3: Glide, version 6.4; Schrödinger, LLC: New York, 2014.

[33] R.A. Friesner, R.B. Murphy, M.P. Repasky, L.L. Frye, J.R. Greenwood, T.A. Halgren, P.C. Sanschagrin, D.T. Mainz, Extra precision glide: Docking and scoring incorporating a model of hydrophobic enclosure for protein-ligand complexes, J. Med. Chem., 49 (2006) 6177-6196.

[34] H.F. Huang, R. Chopra, G.L. Verdine, S.C. Harrison, Structure of a covalently trapped catalytic complex of HIV-I reverse transcriptase: Implications for drug resistance, Science, 282 (1998) 1669-1675.

[35] S.G. Sarafianos, K. Das, C. Tantillo, A.D. Clark, J. Ding, J.M. Whitcomb, P.L. Boyer, S.H. Hughes, E. Arnold, Crystal structure of HIV-1 reverse transcriptase in complex with a polypurine tract RNA : DNA, EMBO J., 20 (2001) 1449-1461.

[36] S.G. Sarafianos, A.D. Clark, K. Das, S. Tuske, J.J. Birktoft, P. Ilankumaran, A.R. Ramesha,

J.M. Sayer, D.M. Jerina, P.L. Boyer, S.H. Hughes, E. Arnold, Structures of HIV-1 reverse transcriptase with pre- and post-translocation AZTMP-terminated DNA, EMBO J., 21 (2002) 6614-6624.

[37] http://www.rcsb.org/pdb/explore/explore.do?structureId=5J1E.

[38] K.A. Kirby, H.A. Schmidt, A.D. Huber, S. Kim, R.K. Rao, S.T. Kramer, Q. Yang, K. Singh, S.G. Sarafianos, K.A. Kirby, R.K. Rao, Q. Yang, K. Singh, S.G. Sarafianos, N.A. Myshakina, M.A. Parniak, N.A. Myshakina, M.T. Christen, Z. Xi, R. Ishima, Y.-L. Chen, Z. Wang, H.A. Schmidt, A.D. Huber, S. Kim, S.T. Kramer, S.G. Sarafianos, A 2-hydroxyisoquinoline-1,3-dione active site RNase H inhibitor binds in multiple modes to HIV-1 reverse transcriptase, Antimicrob Agents Chemother., (2017 Epub July 31).

[39] R.S. Fletcher, G. Holleschak, E. Nagy, D. Arion, G. Borkow, Z.X. Gu, M.A. Wainberg, M.A.

Parniak, Single-step purification of recombinant wild-type and mutant HIV-1 reverse transcriptase, Protein Expr. Purif., 7 (1996) 27-32.

[40] M.A. Parniak, K.L. Min, S.R. Budihas, S.F.J. Le Grice, J.A. Beutler, A fluorescence-based high-throughput screening assay for inhibitors of human immunodeficiency virus-1 reverse transcriptase-associated ribonuclease H activity, Anal. Biochem., 322 (2003) 33-39.

[41] S.K.V. Vernekar, J. Tang, B. Wu, A.D. Huber, M.C. Casey, N. Myshakina, D.J. Wilson, J. Kankanala, K.A. Kirby, M.A. Parniak, S.G. Sarafianos, Z. Wang, Double-winged 3-hydroxypyrimidine-2,4-diones: potent and selective inhibition against HIV-1 RNase H with significant antiviral activity, J. Med. Chem., 60 (2017) 5045-5056.

[42] Z.Q. Wang, E.M. Bennett, D.J. Wilson, C. Salomon, R. Vince, Rationally designed dual inhibitors of HIV reverse transcriptase and integrase, J. Med. Chem., 50 (2007) 3416-3419.

[43] M.E. Abram, M.A. Parniak, Virion instability of human immunodeficiency virus type 1 reverse transcriptase (RT) mutated in the protease cleavage site between RT p51 and the RT RNase H domain, J. Virol., 79 (2005) 11952-11961.

[44] G.M. Sastry, M. Adzhigirey, T. Day, R. Annabhimoju, W. Sherman, Protein and ligand preparation: parameters, protocols, and influence on virtual screening enrichments, J. Comput. Aided Mol. Des, 27 (2013) 221-234.

[45] Schrödinger Release 2014-3: Schrödinger Suite 2014-3 Protein Preparation Wizard; Epik version 2.9, Schrödinger, LLC, New York, NY, 2014; Impact version 6.4, Schrödinger, LLC, New York, NY, 2014; Prime version 3.7, Schrödinger, LLC, New York, NY, 2014.

[46] W.L. Jorgensen, D.S. Maxwell, J. TiradoRives, Development and testing of the OPLS all-atom force field on conformational energetics and properties of organic liquids, J. Am. Chem. Soc., 118 (1996) 11225-11236.

[47] Schrödinger Release 2014-3: LigPrep, version 3.1, Schrödinger, LLC, New York, NY, 2014.

[48] K.A. Kirby, B. Marchand, Y.T. Ong, T.P. Ndongwe, A. Hachiya, E. Michailidis, M.D. Leslie,

D.V. Sietsema, T.L. Fetterly, C.A. Dorst, K. Singh, Z.Q. Wang, M.A. Parniak, S.G. Sarafianos, Structural and inhibition studies of the RNase H function of xenotropic murine leukemia virus-related virus reverse transcriptase, Antimicrob Agents Chemother., 56 (2012) 2048-2061.

[49] J.D. Bauman, K. Das, W.C. Ho, M. Baweja, D.M. Himmel, A.D. Clark, D.A. Oren, P.L. Boyer, S.H. Hughes, A.J. Shatkin, E. Arnold, Crystal engineering of HIV-1 reverse transcriptase for structure-based drug design, Nucleic Acids Res., 36 (2008) 5083-5092.

[50] G. Winter, C.M.C. Lobley, S.M. Prince, Decision making in xia2, Acta Crystallogr. D Biol. Crystallogr., 69 (2013) 1260-1273.

[51] W. Kabsch, XDS, Acta Crystallogr. D Biol. Crystallogr., 66 (2010) 125-132.

[52] B.W. Matthews, Determination of protein molecular-weight, hydration, and packing from crystal density, Methods Enzymol., 114 (1985) 176-187.

[53] M.D. Winn, C.C. Ballard, K.D. Cowtan, E.J. Dodson, P. Emsley, P.R. Evans, R.M. Keegan, E.B. Krissinel, A.G.W. Leslie, A. McCoy, S.J. McNicholas, G.N. Murshudov, N.S. Pannu, E.A. Potterton, H.R. Powell, R.J. Read, A. Vagin, K.S. Wilson, Overview of the CCP4 suite and current developments, Acta Crystallogr. D Biol. Crystallogr., 67 (2011) 235-242.

[54] R.M. Keegan, M.D. Winn, MrBUMP: an automated pipeline for molecular replacement, Acta

Crystallogr. D Biol. Crystallogr., 64 (2008) 119-124.

[55] J.D. Bauman, D. Patel, C. Dharia, M.W. Fromer, S. Ahmed, Y. Frenkel, R.S.K. Vijayan, J.T.

Eck, W.C. Ho, K. Das, A.J. Shatkin, E. Arnold, Detecting allosteric sites of HIV-1 reverse transcriptase by X-ray crystallographic fragment screening, J. Med. Chem., 56 (2013) 2738-2746.

[56] K. Cowtan, The Buccaneer software for automated model building. 1. Tracing protein chains,

Acta Crystallogr. D Biol. Crystallogr., 62 (2006) 1002-1011.

[57] K. Cowtan, Recent developments in classical density modification, Acta Crystallogr. D Biol.

Crystallogr., 66 (2010) 470-478.

[58] P. Emsley, B. Lohkamp, W.G. Scott, K. Cowtan, Features and development of Coot, Acta Crystallogr. D Biol. Crystallogr., 66 (2010) 486-501.

[59] P.D. Adams, P.V. Afonine, G. Bunkoczi, V.B. Chen, I.W. Davis, N. Echols, J.J. Headd, L.W. Hung, G.J. Kapral, R.W. Grosse-Kunstleve, A.J. McCoy, N.W. Moriarty, R. Oeffner, R.J. Read, D.C. Richardson, J.S. Richardson, T.C. Terwilliger, P.H. Zwart, PHENIX: a comprehensive Python-based system for macromolecular structure solution, Acta Crystallogr. D Biol. Crystallogr., 66 (2010) 213-221.

[60] N.S. Pannu, G.N. Murshudov, E.J. Dodson, R.J. Read, Incorporation of prior phase information strengthens maximum-likelihood structure refinement, Acta Crystallogr. D Biol. Crystallogr., 54 (1998) 1285-1294.

[61] G.N. Murshudov, P. Skubak, A.A. Lebedev, N.S. Pannu, R.A. Steiner, R.A. Nicholls, M.D. Winn, F. Long, A.A. Vagin, REFMAC5 for the refinement of macromolecular crystal structures, Acta Crystallogr. D Biol. Crystallogr., 67 (2011) 355-367.

[62] V.B. Chen, W.B. Arendall, J.J. Headd, D.A. Keedy, R.M. Immormino, G.J. Kapral, L.W. Murray, J.S. Richardson, D.C. Richardson, MolProbity: all-atom structure validation for macromolecular crystallography, Acta Crystallogr. D Biol. Crystallogr., 66 (2010) 12-21.

**Highlights**

- Design of high potency novel inhibitors of HIV RT-associated RNase H activity.
- Efficient synthesis of N-Hydroxy thienopyrimidine-2,4-dione derivatives.
- Generally selective RNase H inhibition over INST and RT Pol.
- Compound **11d** exhibited significant inhibitory activity in a cell-based antiviral assay with an $EC_{50}$ of 7.4 µM.
- Crystallographic and molecular modeling studies corroborated the RNase H active site binding mode.

**Captions of Figures, Schemes and Table**

**Figure 1.** Design of active site RNase H inhibitors. (A) Major chemotypes reported as HIV RNase H active site inhibitors. All chemotypes contain a chelating triad (magenta); scaffolds **4**–**7** also feature an aryl or biaryl moiety (cyan) connected through a methylene or amino linker; (B) N-hydroxyurea (blue) chemotype **9** is designed based on reported HID (**2**) and HPD (**8**) chemotypes. Bioisosteric replacement of **9** allows the further design of inhibitor types **10–11**.

**Figure 2.** Molecular modeling of analogues **11a** and **11d** at the RNase H active site. (A) Predicted binding mode of **11a** (Green) within active site of RNase H (PDB code 5J1E) [15, 37]. Active site residues are highlighted in yellow sticks with metal ions as magenta spheres, water molecules (W1 and W2) as red spheres. Chelating and H-bond interactions are depicted as black dotted lines. (B) Predicted binding modes of **11d** (Magenta) within active site of RNase H. π-stack interaction is highlighted with a black double headed arrow. (C) Alternative predicted binding mode (low scoring) of **11d** (Blue) within active site of RNase H. (D) Glide XP docking scores for compounds **11a** and **11d**.

**Figure 3.** Crystal structure of HIV-1 RT in complex with **11b**. There are two unique RT molecules in the crystal structure (RT1 and RT2, middle panel; the p66 subunit of RT1 is shown in orange and the p66 subunit of RT2 is shown in green; p51 subunits are shown in gray). A zoomed in, cross-eyed stereo view image of the RNase H active site of RT1 is shown in the top panel (**11b** shown in cyan sticks), while a zoomed in, cross-eyed stereo view image of the RNase H active site of RT2 is shown in the bottom panel (**11b** shown in pink sticks). Conserved active site residues are shown in sticks, $Mn^{2+}$ ions are shown as purple spheres, and water molecules

(W1 and W2 in top panel; W3 and W4 in bottom panel) chelating the $Mn^{2+}$ ions are shown as red spheres. Metal chelating interactions are shown as black dotted lines and interactions between **11b** and RT are shown as red dotted lines.

**Scheme 1**[a] Synthesis of **14**, **9**, **19**, and **10**.

**Scheme 2**[a] Synthesis of chemotype **11.**

**Table 1**. Biochemical and antiviral assay results of chemotypes **9–11.**

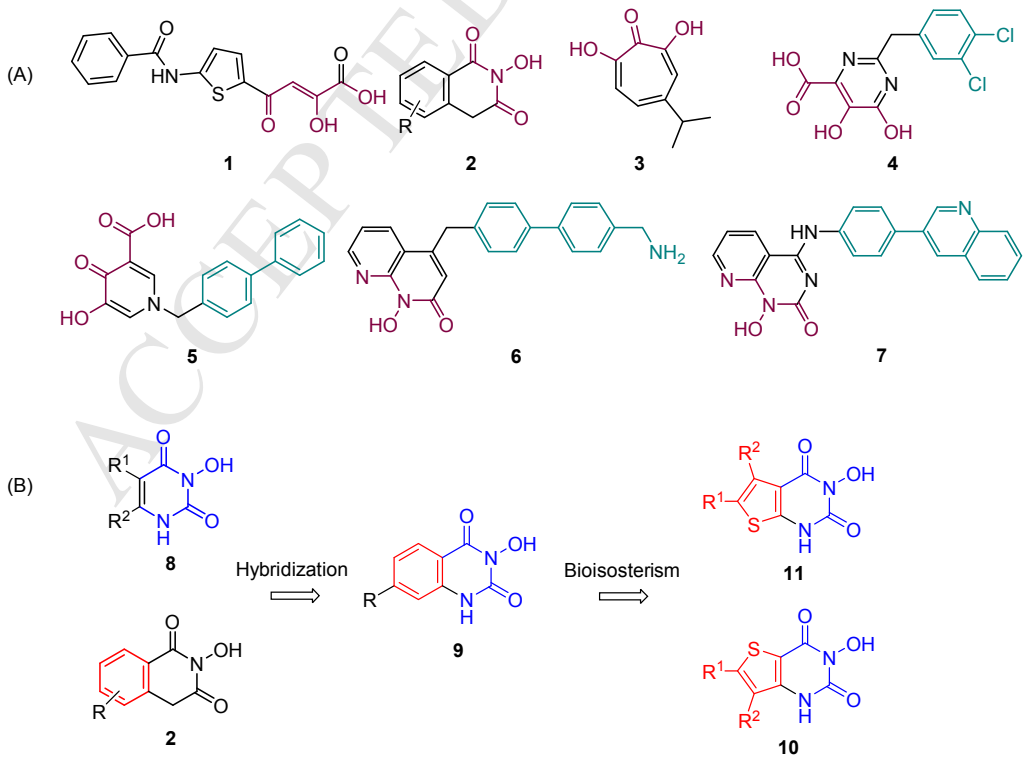

**Figure 1.** Design of active site RNase H inhibitors. (A) Major chemotypes reported as HIV RNase H active site inhibitors. All chemotypes contain a chelating triad (magenta); scaffolds **4**–**7** also feature an aryl or biaryl moiety (cyan) connected through a methylene or amino linker; (B) N-hydroxyurea (blue) chemotype **9** is designed based on reported HID (**2**) and HPD (**8**) chemotypes. Bioisosteric replacement of **9** allows the further design of inhibitor types **10–11**.

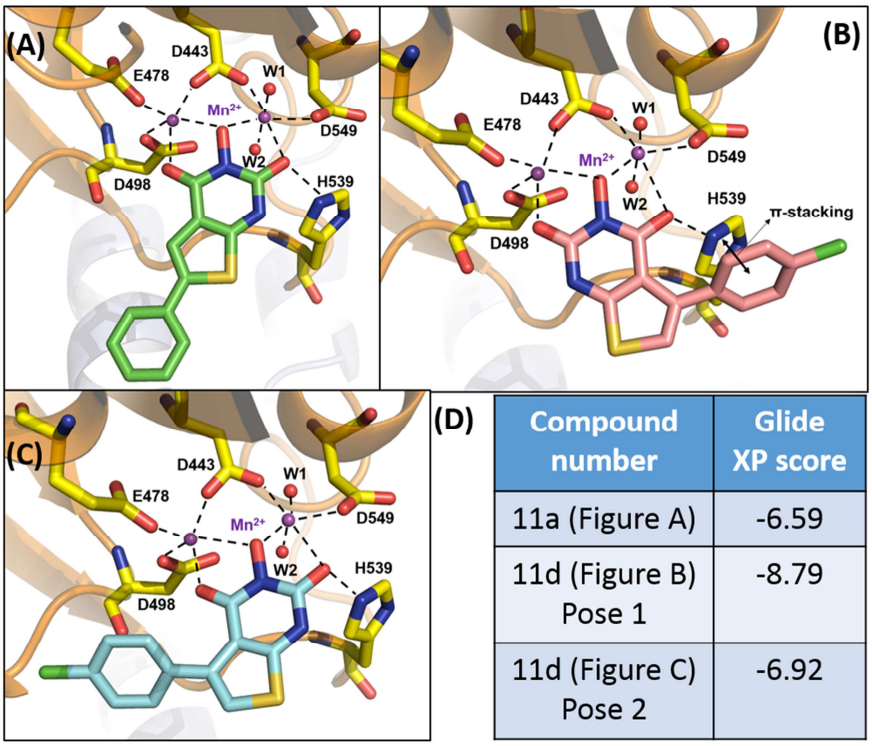


(D)

| Compound number | Glide XP score |
|---|---|
| 11a (Figure A) | -6.59 |
| 11d (Figure B) Pose 1 | -8.79 |
| 11d (Figure C) Pose 2 | -6.92 |

**Figure 2.** Molecular modeling of analogues **11a** and **11d** at the RNase H active site. (A) Predicted binding mode of **11a** (Green) within active site of RNase H (PDB code 5J1E) [15, 37]. Active site residues are highlighted in yellow sticks with metal ions as magenta spheres, water molecules (W1 and W2) as red spheres. Chelating and H-bond interactions are depicted as black dotted lines. (B) Predicted binding modes of **11d** (Magenta) within active site of RNase H. π-stack interaction is highlighted with a black double headed arrow. (C) Alternative predicted binding mode (low scoring) of **11d** (Blue) within active site of RNase H. (D) Glide XP docking scores for compounds **11a** and **11d**.

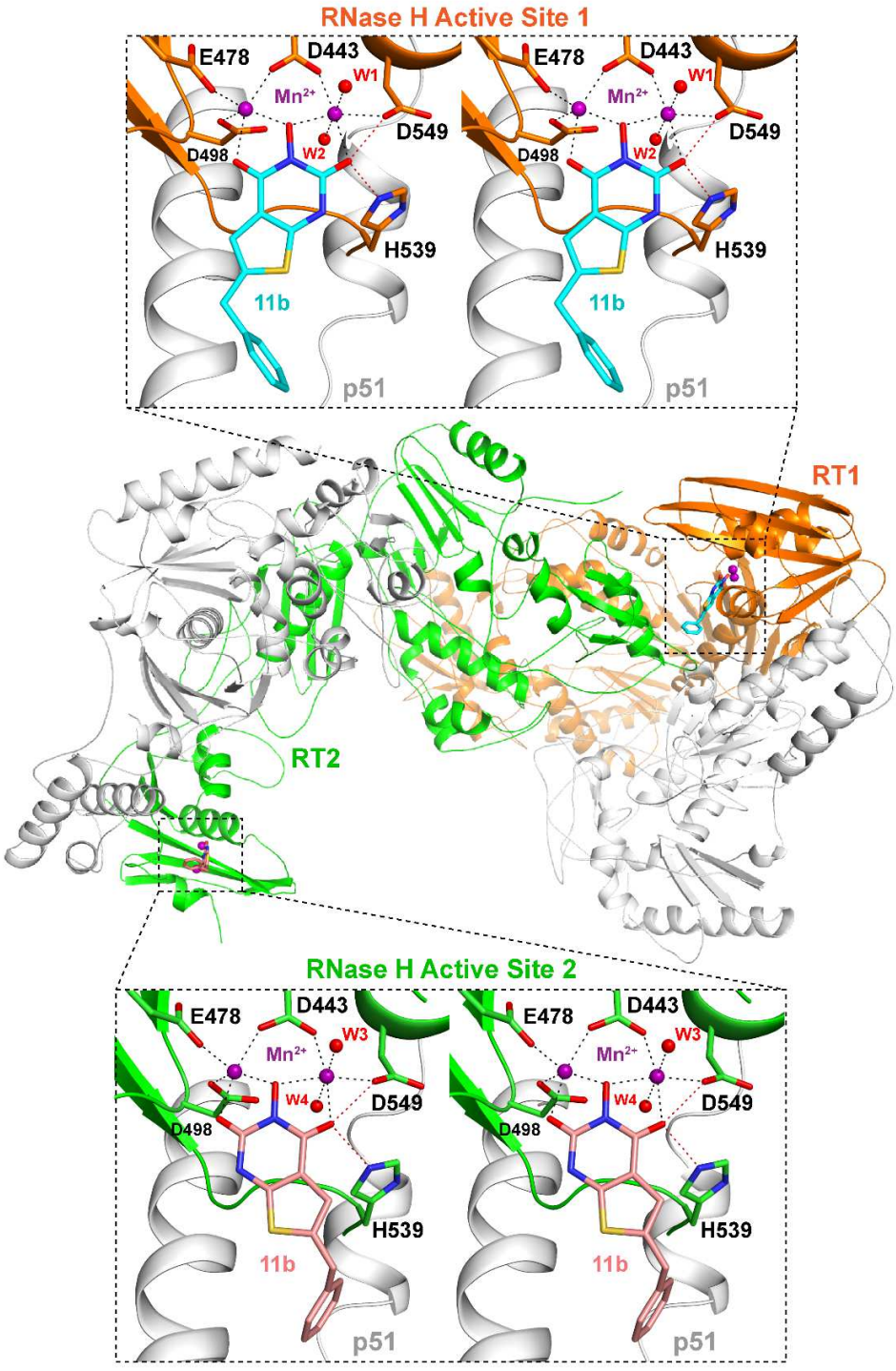


**Figure 3.** Crystal structure of HIV-1 RT in complex with **11b**. There are two unique RT molecules in the crystal structure (RT1 and RT2, middle panel; the p66 subunit of RT1 is shown in orange and the p66 subunit of RT2 is shown in green; p51 subunits are shown in gray). A

zoomed in, cross-eyed stereo view image of the RNase H active site of RT1 is shown in the top panel (**11b** shown in cyan sticks), while a zoomed in, cross-eyed stereo view image of the RNase H active site of RT2 is shown in the bottom panel (**11b** shown in pink sticks). Conserved active site residues are shown in sticks, $Mn^{2+}$ ions are shown as purple spheres, and water molecules (W1 and W2 in top panel; W3 and W4 in bottom panel) chelating the $Mn^{2+}$ ions are shown as red spheres. Metal chelating interactions are shown as black dotted lines and interactions between **11b** and RT are shown as red dotted lines.

**Scheme 1**[a] Synthesis of **14**, **9**, **19**, and **10**.

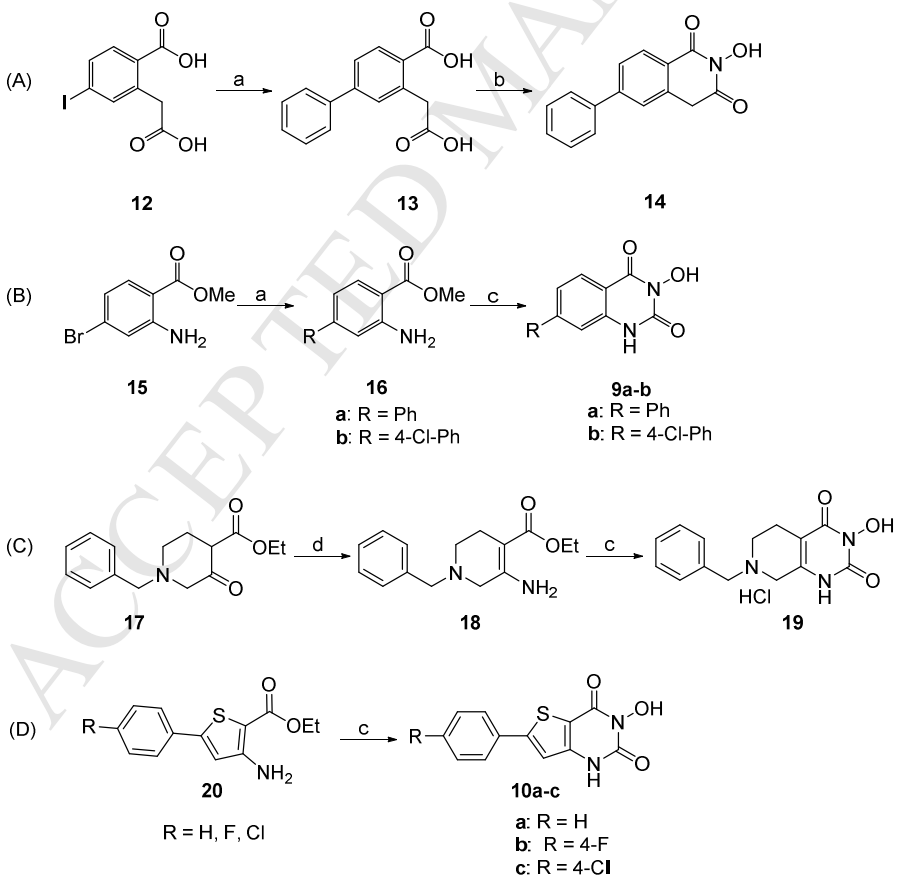

[a] Reagents and conditions: (a) arylboronic acid, $K_2CO_3$, $Pd(PPh_3)_4$, EtOH/$H_2O$ (1:1), 150 °C, 30 min, MW, 50-71%; (b) (i) $NH_2OTHP$, CDI, toluene, reflux, 12 h; (ii) p-TSA hydrate, MeOH, 2−3 h, rt; 69% (c) (i) CDI, toluene, reflux then $H_2NOPG$; (b) aq NaOH, EtOH, refluxt; (c) p-TSA hydrate, MeOH, 2−3 h, rt or HBr in acetic acid; 40-85% (d) $NH_4OAc$, EtOH, r.t, 75%.

**Scheme 2**[a] Synthesis of chemotype **11**

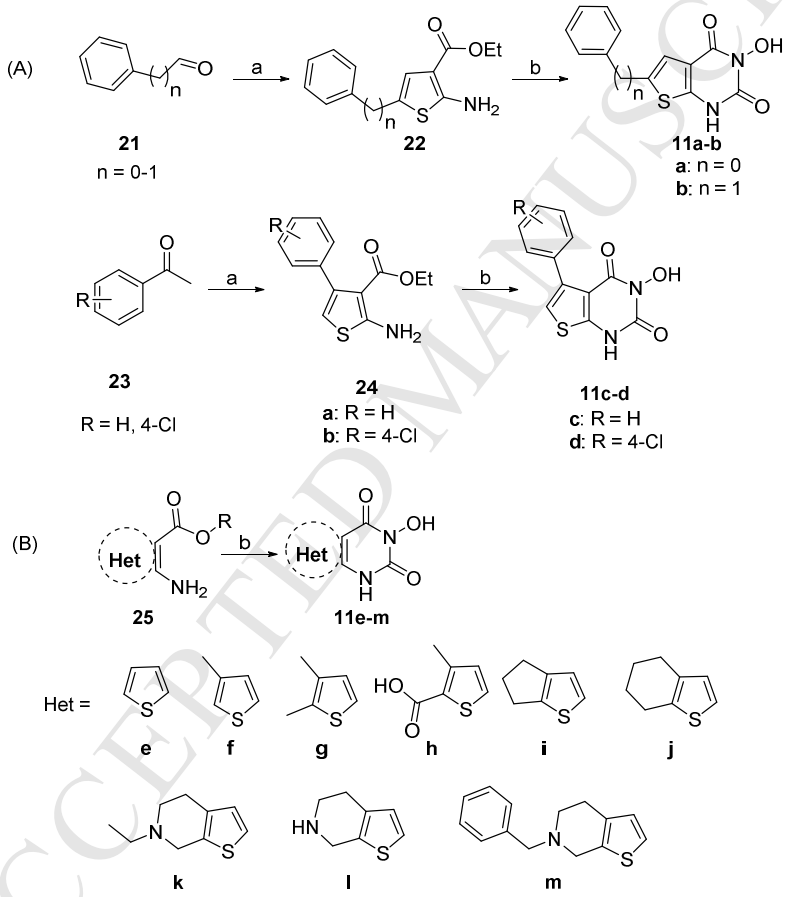


[a] Reagents and conditions: (a) ethyl cyanoacetate, $S_8$, morpholine, 120 °C, MW, 53-82%; (b) p-TSA hydrate, MeOH, 2−3 h, rt or HBr in acetic acid, 48-85%.

**Table 1**. Biochemical and antiviral assay results of chemotypes **9**–**11**

| Compd | Structure | RT $IC_{50}$ [a] (μM) | | INST $IC_{50}$ [a] (μM) | MAGI Antiviral | |
|---|---|---|---|---|---|---|
| | | RNase H | Pol | | $EC_{50}$ [b] (μM) | $CC_{50}$ [c] (μM) |
| **14** | 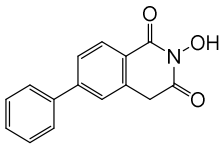 | 1.3 ± 0.8 | >10 | 2.0 ± 0.4 | 16 ± 2 | 19 ± 3 |
| **9a** | 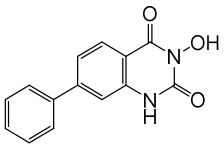 | 0.20 ± 0.1 | >10 | 11 ± 3 | 3.8 ± 0.1 | 6.0 ± 0.2 |
| **9b** | 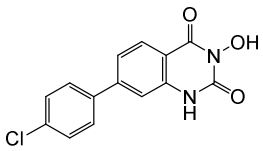 | 0.20 ± 0.1 | >10 | NA | 4.5 ± 0.7 | 9.9 ± 0.3 |
| **19** | 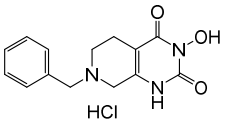 | 0.33 ± 0.05 | >10 | >100 | >20 | 96 ± 0.1 |
| **10a** | 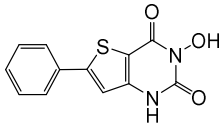 | 0.10 ± 0.06 | >10 | 4.5 ± 0.8 | 11 ± 2 | 28 ± 0.2 |
| **10b** | 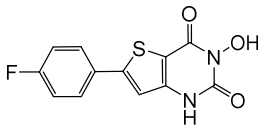 | 0.20 ± 0.1 | >10 | 17 ± 4 | >20 | >100 |
| **10c** | 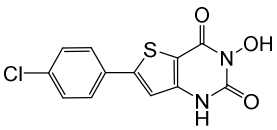 | 0.070 ± 0.05 | >10 | 23 ± 6 | >20 | >100 |
| **11a** | 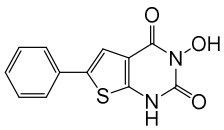 | 0.084 ± 0.006 | >10 | 2.2 ± 0.4 | >20 | >100 |

| | | | | | | |
|---|---|---|---|---|---|---|
| **11b** | 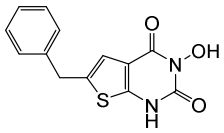 | 0.043 ± 0.008 | >10 | 5.0 ± 1 | >20 | >100 |
| **11c** | 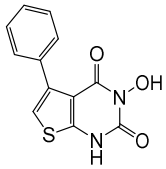 | 0.10 ± 0.03 | >10 | 1.3 ± 0.1 | 14 ± 1 | >100 |
| **11d** | 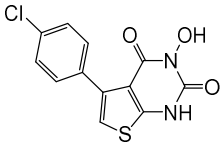 | 0.040 ± 0.02 | >10 | 2.1 ± 0.3 | 7.4 ± 0.3 | >100 |
| **11e** | 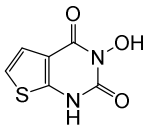 | 0.20 ± 0.03 | >10 | 35 ± 6 | 18 ± 1 | 54 ± 6 |
| **11f** | 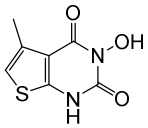 | 0.10 ± 0.02 | >10 | 12 ± 2 | >20 | 81 ± 6 |
| **11g** | 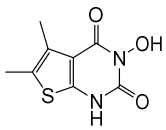 | 0.10 ± 0.03 | >10 | 8.4 ± 1 | 8.9 ± 1 | 62 ± 1 |
| **11h** | 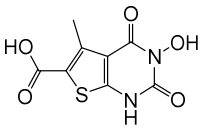 | 0.10 ± 0.02 | >10 | 7.9 ± 1 | >20 | >100 |
| **11i** | 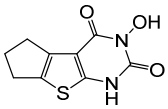 | 0.10 ± 0.03 | >10 | 5.6 ± 0.5 | 22 ± 4 | >100 |
| **11j** | 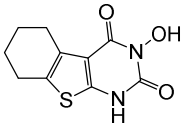 | 0.10 ± 0.02 | >10 | 3.6 ± 0.5 | 21 ± 1 | >100 |
| **11k** | 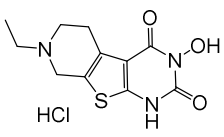 | 0.20 ± 0.03 | >10 | >100 | >20 | >100 |

| | | | | | | |
|---|---|---|---|---|---|---|
| **11l** | 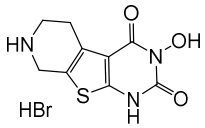 | 0.30 ± 0.03 | >10 | 17 ± 3 | >20 | >100 |
| **11m** | 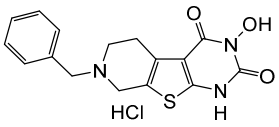 | 0.10 ± 0.04 | >10 | 8.3 ± 0.8 | >20 | >100 |
| **RAL**[d] | -- | >10 | ND[e] | 0.65 | 0.030 ± 0.005 | ND |

[a] Concentration of compound inhibiting the target enzyme by 50%. [b] Concentration of compound inhibiting virus replication by 50%. [c] Concentration of compound resulting in 50% cell death. [d] RAL = raltegravir; [e] ND = not determined. All assay results expressed as mean ± standard deviation from at least two independent experiments.